Three-micron imaging of the Hubble Deep Field[1]

David W. Hogg,[2,3] Gerry Neugebauer,[4] Judith G. Cohen,[4] Mark Dickinson,[5] S. G. Djorgovski,[4] Keith Matthews,[4] B. T. Soifer[4]

ABSTRACT

Images of the Hubble Deep Field at 3.2 μm, taken with the 10-m Keck Telescope, are presented. The images cover a total area of ~ 2.5 arcmin^2. To a 5-sigma limit of $[3.2]_{total} \approx 17.5$ mag (Vega-relative), 11 sources are detected, 9 of which are extragalactic. The integrated galaxy number counts are therefore $\sim 1.3 \times 10^4$ deg^{-2} to this depth. The galaxies detected at 3.2 μm have a median redshift of $z = 0.56$. All 3.2 μm sources have 1.6 μm, 1.1 μm and visual counterparts, all of fairly regular morphologies; several also have 6.7 μm, 15 μm, 850 μm, 8.5 GHz, or 1.4 GHz counterparts. No sources are found which are either anomalously red or anomalously blue in their $H - [3.2]$ color, and there are significant detections of most of the known near-infrared HDF sources for which detection in these 3.2 μm data seemed likely.

Subject headings: galaxies: photometry — galaxies: statistics — infrared: galaxies — techniques: photometric

1. Introduction

Until now, it has been impractical to make wide-field ground-based surveys at infrared wavelengths longer than 2.4 μm. Although the atmosphere is transparent in wavelength windows in the near infrared out to 10 μm, sky brightness increases rapidly with increasing wavelength. Detector area is limited by the need to read out quickly before saturation. The Near Infrared Camera (NIRC; Matthews & Soifer 1994) on the 10-m W. M. Keck Telescope, however, is equipped with a fast readout mode which allows it to read out its entire array quickly enough to avoid saturation in a short-wavelength L-band filter, centered on 3.2 μm.

[2] Institute for Advanced Study, Olden Lane, Princeton NJ 08540, USA; `hogg@ias.edu`

[3] Hubble Fellow

[4] Palomar Observatory, California Institute of Technology, mail code 105-24, Pasadena CA 91125, USA

[5] Space Telescope Science Institute, 3700 San Martin Drive, Baltimore MD 21218, USA

The 3.2 μm bandpass is complementary to the standard near-infrared J, H, and K (1.2, 1.6 and 2.2 μm) bandpasses in a number of respects. It admits light at the rest-frame wavelengths of these bandpasses at redshifts of 1.7, 1.0, and 0.5, so observations of intermediate and high-redshift galaxies can be compared directly to local analogs observed in the standard bandpasses. The 3.2 μm bandpass can be used to extend the near-infrared spectral energy distributions (SEDs) to longer wavelengths. While stellar populations are made up of a superposition of basically thermal radiators, nuclear activity tends to be redder than thermal (in the near infrared, bluer in the visual) and thus ought to become more prominent in redder bandpasses. Nuclear activity may also heat nuclear dust to produce additional near-infrared emission (eg, Peletier et al 1999). In units of f_ν, the SEDs of normal galaxies peak at ≈ 1.6 μm, primarily due to a minimum in H^- opacity in stellar atmospheres. At $z = 1$, this peak is redshifted to 3.2 μm. A "non-evolving" L^* elliptical galaxy at redshift $z = 1$ ought to appear as a ~ 17.5 mag source at 3.2 μm. At $z = 1$, old stellar populations are 1.5 to 3 mag brighter than young stellar populations with the same apparent V magnitude (Coleman et al 1980, Aaronson 1977).

This paper presents the results of deep imaging of the Hubble Deep Field (HDF; Williams et al 1996) in the 3.2 μm bandpass with NIRC. Although neither the sky coverage nor the number of detected sources is large, to our knowledge this is the first deep near-infrared survey at wavelengths beyond the K band. It extends the SEDs of HDF sources over a decade in wavelength from the F300W bandpass at 0.3 μm. The choice of the HDF for deep imaging in this new 3.2 μm bandpass was clear: The HDF is currently the most well-studied field on the sky, deeply imaged by almost every astronomical technique.

In what follows, all magnitudes are Vega-relative.

2.   Observations and reduction

The L_{short} filter on NIRC was chosen for this study. The filter passes light in the wavelength range $2.5 < \lambda < 3.5$ μm. When combined with typical atmospheric absorption conditions on Mauna Kea, the bandpass is concentrated in the wavelength range $2.9 < \lambda < 3.5$ μm, with a small "blue leak" (~ 10 percent of the total transmission function) in a narrow peak at 2.5 μm. The central wavelength is ~ 3.2 μm for the filter plus atmosphere transmission function; for this reason, magnitudes with this instrument and filter setup will be denoted [3.2]. The L_{short} filter is currently the longest-wavelength bandpass in which NIRC can read out its full 256×256 pixel (38×38 arcsec^2) field area without saturation from sky brightness alone. A source with $[3.2] = 0$ mag in the L_{short} bandpass has a flux density of 330 Jy. This approximate zeropoint is an interpolation between measured K and L-band zeropoints, and is uncertain by no more than 10 percent.

The selection of the HDF for deep study with HST is described elsewhere (Williams et al 1996). Within the HST-imaged portion of the HDF, a set of subfields were chosen for deep study

with NIRC. These subfields were not chosen with regard to any particular "interesting sources." Rather, one subfield was chosen to lie roughly in the center of each WFPC2 CCD chip image, subject to guide star constraints (these are the primary subfields A, B, C, and D), and additional subfields were chosen to fill in the gaps between these four primary subfields. In the end, telescope time and weather restricted our study to five subfields, the primary four and subfield F, which lies between subfields C and D. The well-observed solid angle is roughly 0.5 arcmin^2 per subfield (given dithering) or a total of 2.5 arcmin^2. The layout of the subfields is shown in Figure 1, relative to the HST-imaged field.

Air mass of the observations ranged from 1.40 to 1.75. The conditions were clear and apparently photometric for all nights, although there was some variation in the sky brightness. Each individual exposure consisted of 1000 (or, occasionally, 2000) 0.025 s or 0.029 s integrations coadded into a single image in hardware. A visual imaging offset guider pointing at a star maintained the tracking of the telescope. The observations were taken in half-hour or hour-long sets with random dithers over a 10×10 arcsec^2 range. The photometric sensitivity was determined by measuring faint standard stars (Elias et al 1982, Persson et al 1998) roughly once per hour during each night. During several of the nights, the measured sensitivity (corrected for airmass) varied in an apparently linear way with time. The subfield most affected by this was subfield A, which shows no significant sources (see below), so the variation in this subfield does not affect the results. The scatter of the individual standard-star measurements around the linear sensitivity trends is ± 0.05 mag, but for the other four subfields, the trends themselves range between $\pm < 0.01$ mag for subfield D and ± 0.12 mag for subfield F. The uncertainty in the photometric calibration is thus no better than 0.05 mag, but may be worse if the linear trends represent a serious photometric problem. The observing dates, integration times, and sensitivities of the final, stacked images of the subfields are given in Table 1.

The data were processed by subtracting an average of the two adjacent images (before and after) from each image to eliminate artifacts introduced by varying sky brightness and field rotation resulting from the alt–azimuth configuration of the Keck Telescope. Because the individual images show no significant sources above the sky noise, registration of the individual images was accomplished with telescope coordinates as computed from the positions of the star in the guider camera. The individual registered images were averaged, after dark subtraction and flat-fielding, to produce the final images shown in Fig 1. The pixel-to-pixel rms values in the central parts of the images correspond to ≈ 20.2 mag in 1 arcsec^2; the specific values for each subfield are given in Table 1.

Because there are so few sources visible per subfield (none for subfield A), determination of the seeing is difficult. Seeing values given in Table 1 are determined by comparison of the sources in the final, stacked images to their visual counterparts in the WFPC2 image of the HDF taken in the F814W bandpass (Williams et al 1996); they are necessarily quite uncertain. Since in several fields (especially F) the seeing in the final, stacked image is apparently worse than that for the standard stars, some of the seeing must arise from poor registration of the frames coadded in the

stacks.

For visual images, the "version 2" reductions of the HST/WFPC2 imaging of the HDF were used. Details of the data acquisition, reduction, and sensitivities are given elsewhere (Williams et al 1996). For brevity, the F300W, F450W, F606W, and F814W bandpasses will be referred-to here as U, B, V, and I, although F300W and F606W are substantially different from conventional U and V.

For other near-infrared data, the "version 1.04" reductions of the imaging of the HDF taken with the NICMOS instrument on HST were used. Details of the data acquisition, reduction, and sensitivities are given elsewhere (Dickinson et al 2000). For brevity, the F110W and F160W bandpasses will be referred-to here as J and H, although F110W is substantially bluer than standard J. The photometric sensitivities of the J and H data are uncertain at the ~ 5 percent level.

3.   Source selection and photometry

Sources were identified in the 3.2 μm image by requiring a positive deviation of greater significance than $5.0\,\sigma$ inside a focal-plane aperture of 1.0 arcsec diameter in the final, stacked images of the subfields. The $1\,\sigma$ noise levels were estimated by measuring fluxes in randomly placed apertures, so they correctly take into account any pixel-to-pixel correlations. At significances less than $10\,\sigma$, it was established that the sources had visual and near-infrared counterparts in the HST images. No $5.0\,\sigma$ deviations failed to show counterparts, except at the very edges of the subfields, where the noise and background flatness are degraded. A total of 11 sources were selected. The total area subject to source detection is roughly 2.5 arcmin^2.

Total magnitudes $[3.2]_{\mathrm{total}}$ for the sources selected at 3.2 μm were estimated by measuring aperture magnitudes $[3.2]_{\mathrm{ap}}$ in focal-plane apertures of 2.0 arcsec diameter and then correcting for the small size of the aperture. The 2.0 arcsec aperture was chosen to be small enough to reduce the background at 3.2 μm but large enough to reduce variations in photometric sensitivity measured from the standard stars to below 0.1 mag. The aperture corrections were determined under the assumption that there are only small color gradients in $(H - [3.2])$ color, by comparing 2.0 and 6.0 arcsec diameter aperture magnitudes in the very high signal-to-noise H-band image, smoothed to the seeing of the 3.2 μm image. (The one exception is the star at $12\,36\,56.368\ +62\,12\,41.14$, for which a 5.0 arcsec diameter aperture was used in order to avoid light from the neighboring bright galaxy.) Aperture and total magnitudes for the sources are given in Table 2. The uncertainties given in Table 2 are based only on the photon statistics and the uncertainties in determining the sky level, and do not include uncertainties in the photometric sensitivity. No estimate is made for the uncertainties in the aperture corrections. These may be considerable, if the seeing estimates are in error, if there are significant color gradients, or if there is significant light outside of the 6.0 arcsec diameter aperture.

Colors were measured in 2.0 arcsec diameter focal-plane apertures in the visual WFPC2 and near-infrared NICMOS images, smoothed to the seeing of the 3.2 μm images. The aperture size was chosen so the colors were measured in the regions of the sources which are well-measured at 3.2 μm. The colors are given in Table 3. The photon and read-noise contributions to the uncertainties in the color measurements are at or below the 0.01 mag level for the all the visual and near-infrared colors except for $(H - [3.2])$ where the uncertainties are dominated by the uncertainty in $[3.2]_{\mathrm{ap}}$ given in Table 2 and $(U - B)$ where the uncertainties are at the 0.01 to 0.2 mag level, depending on U-band flux. Although the NICMOS J and H measurements have a very high signal-to-noise ratio, the photometric sensitivities are uncertain at the ~ 10 percent level (Dickinson et al 2000). Figure 2 shows $(V - [3.2])$ and $(H - [3.2])$ colors for the galaxies as a function of redshift. Figure 3 shows the visual and near-infrared counterparts of all the sources.

Absolute RA and Dec positions were assigned to the sources under the assumption that the absolute astrometry of the visual HST images of the HDF (Williams et al 1996) is correct. These absolute positions are given in Table 2.

4. Comparison with other HDF catalogs

The catalog selected at 3.2 μm can be compared with other catalogs made in the HDF at other wavelengths or with other techniques. The redshifts and flux densities at other wavelengths discussed in this Section are presented in Tables 3 and 4.

Redshifts were found by comparing the coordinates of the sources with the lists of redshifts obtained in the Hubble Deep Field with the Keck Telescope (Cohen et al 1996; Lowenthal et al 1997; Cohen et al 2000). Two of the sources are Galactic stars, consistent with their stellar appearance on the HST images.

Flux densities in the K_s band (2.15 μm) were found by matching the absolute positions of the 3.2 μm sources with the positions of the sources from the K_s-selected catalog of Hogg et al (2000). Flux densities at 6.7 and 15 μm were found by matching with the catalogs made from imaging data from the Infrared Space Observatory (Aussel et al 1999; based on data from Serjeant et al 1997). Flux densities at 850 μm were taken from the catalog made from the SCUBA instrument at JCMT (Hughes et al 1998), although the sources were identified in part through comparing positions derived from 1.4 GHz observations (Richards 1999a). Flux densities at 8.5 and 1.4 GHz were found by matching positions in catalogs made with VLA data at these frequencies (Richards et al 1998; Richards 1999b).

The detection fraction at 3.2 μm of known near-infrared sources was tested by identifying sources in the NICMOS/HDF catalogs (Dickinson et al 2000) satisfying

$$[3.2]_{\mathrm{predicted}} = F160W - 1.85\,(F110W - F160W) + 0.25 < 18 \tag{1}$$

which corresponds to an approximate linear extrapolation (in log-log space) of the J and H

magnitudes to [3.2]. (This equation is roughly appropriate for predicting the fluxes of galaxies and nuclear emission, since both have SEDs which resemble power-laws at 3.2 μm (observed) at the redshifts of interest.) All nine sources inside the region of the HDF well-observed at 3.2 μm with $[3.2]_{predicted} < 17.0$ have counterparts in the catalog selected at 3.2 μm, and of the the six sources in the well-observed region with $17.0 < [3.2]_{predicted} < 18.0$, two have counterparts in the catalog.

5. Results

Images of the Hubble Deep Field at 3.2 μm, taken with the 10-m Keck Telescope were presented, representing the first near-infrared survey of the distant Universe at wavelengths beyond the K band. The images cover a total area of ~ 2.5 arcmin^2.

To a 5-sigma limit of $[3.2]_{total} \approx 17.5$ mag (Vega-relative), 11 sources are detected, 9 of which are extragalactic. The integrated galaxy number counts are therefore $\sim 1.3 \times 10^4$ deg^{-2} to this depth. The sources detected at 3.2 μm have a median redshift of $z = 0.56$.

All 3.2 μm sources have 1.6 μm, 1.1 μm and visual counterparts. No sources are found which are either anomalously red or anomalously blue in their $(V - [3.2])$ or $(H - [3.2])$ colors. In Figure 2, the source colors are compared with no-evolution predictions, based on observations of local galaxies (Coleman et al 1980, Aaronson 1977) and simple models of the filter transmission curves. Although the sources selected at 3.2 μm are among the reddest visually-selected galaxies, they are blue relative to no-evolution predictions. The blue colors are likely a consequence of higher star formation rates at intermediate redshift than in the present-day Universe, as has been inferred, among other ways, from metallicity in Lyman-alpha clouds (Pei & Fall 1995), ultraviolet luminosity density (Lilly et al 1996; Connolly et al 1997; Madau et al 1998) and emission line strengths (Hammer et al 1997; Heyl et al 1997; Small et al 1997; Hogg et al 1998). The lack of very red sources does not constrain the abundance of "extremely red objects" (EROs) because, at the magnitudes of interest, the angular number density of EROs is on the order of 10^{-2} arcmin^{-2} (Hu & Ridgeway 1994; Thompson et al 1999).

The morphologies of the 3.2 μm sources in the visual and near-infrared bandpasses are shown in Figure 3. The sample is small, but they appear fairly regular, with some showing nearby neighbors or evidence for mild interaction.

Comparisons with surveys of the HDF at other wavelengths show that all of the 3.2 μm sources have 2.15 μm counterparts, one has a 6.7 μm counterpart, several have 15 μm counterparts, one has a likely 850 μm counterpart, and two have 8.5 GHz counterparts. Furthermore, there are 3.2 μm detections of the majority of sources which, on the basis of their 1.1 μm and 1.6 μm photometry, ought to have been detected.

In short, the 3.2 μm imaging of the HDF shows no great surprises. It does demonstrate that it is possible, with significant telescope time, to perform studies of normal galaxies at high redshifts

in the L band of atmospheric transmission.

REFERENCES

Aaronson M., 1977, PhD thesis, Harvard University

Aussel H., Cesarsky C. J., Elbaz D., Starck J. L., 1999, A&A 342 313

Cohen J. G., Cowie L. L., Hogg D. W., Songaila A., Blandford R., Hu E. M., Shopbell P., 1996, ApJ 471 L5

Cohen J. G., Hogg D. W., Blandford R. D., Cowie L. L., Hu E., Songaila A., Shopbell P., Richberg K., 2000, ApJS submitted

Coleman G. D., Wu C.-C., Weedman D. W., 1980, ApJS 43 393

Connolly A. J., Szalay A. S., Dickinson M., Subbarao M. U. & Brunner R. J., 1997, ApJ 486 L11

Dickinson M. E., 2000, in preparation

Elias J. H., Frogel J. A., Matthews K., Neugebauer G., 1982, AJ 87 1029

Hammer F., Flores H., Lilly S. J., Crampton D., Le Fèvre O., Rola C., Mallen-Ornelas G., Schade D. & Tresse L., 1997, ApJ 481 49

Heyl J., Colless M., Ellis R. S. & Broadhurst T., 1997, MNRAS 285 613

Hogg D. W., Neugebauer G., Armus L., Matthews K., Pahre M. A., Soifer B. T., Weinberger A. J., 1997, AJ 113 474 (erratum AJ 113 2338)

Hogg D. W., Cohen J. G., Blandford R. & Pahre M. A., 1998, ApJ 504 622

Hogg D. W., Pahre M. A., Adelberger K. L., Blandford R., Cohen J. G., Gautier T. N., Jarrett T., Neugebauer G., Steidel C. C., 2000, ApJS in press

Hu E. M., Ridgeway S. E., 1994, AJ 107 1303

Hughes D. H. et al, 1998, Nature 394 241

Lilly S. J., Le Fèvre O., Hammer F. & Crampton D., 1996, ApJ 460 L1

Lowenthal J. D., Koo D. C., Guzman R., Gallego J., Phillips A. C., Faber S. M., Vogt N. P.,
    Illingworth G. D., Gronwall C., 1997, ApJ 481 673

Madau P., Pozzetti L. & Dickinson M., 1998, ApJ 498 106

Matthews K., Soifer B. T., 1994, in *Infrared Astronomy with Arrays: The Next Generation,*
    Mclean I., ed., Dordrecht: Kluwer, 239

Pei Y. C. & Fall S. M., 1995, ApJ 454 69

Peletier R. F., Knapen J. H., Shlosman I., Pérez-Ramírez D., Nadeau D., Doyon R., Espinosa J.
    M. R., García A. M. P., 1999, astro-ph/9905076

Persson S. E., Murphy D. C., Krzeminski W., Roth M., Rieke M., 1998, AJ 116 2475

Richards E. A., Kellerman K. I., Fomalont E. B., Windhorst R. A., Partridge R. B., 1998, AJ 116
    1039

Richards E. A., 1999a, ApJ 513 L9

Richards E. A., 1999b, ApJ in press

Serjeant S. B. G. et al, 1997, MNRAS 289 457

Small T. A., Sargent W. L. W. & Hamilton D., 1997, ApJ 487 512

Thompson, D. et al., 1999, ApJ 523 100

Williams R. E. et al, 1996, AJ 112 1335

Table 1.   Properties of the final, stacked images of the subfields

name	date (UT)	exposure (s)	seeing FWHM[a] (arcsec)	[3.2] at $1\,\sigma$[b] (mag)
NIRC-HDF-A	1999 April 28	13440	0.5[c]	20.1
NIRC-HDF-B	1998 February 6	11100	0.5	20.4
NIRC-HDF-C	1998 February 7	9600	0.4	20.2
NIRC-HDF-D	1999 April 30	9480	0.4	20.3
NIRC-HDF-F	1999 April 27	11100	0.6	20.0

[a]Because there are so few significant sources per subfield, the seeing measurements are very uncertain; see text.

[b]The $1\,\sigma$ magnitude is that corresponding to a $1\,\sigma$ variation in the sky in a focal-plane aperture of 1 arcsec^2 in solid angle, in the central (i.e., full exposure-time) part of the image.

[c]The seeing FWHM for subfield A is taken from the observations of the standard stars, because there are no significant sources detected in that subfield.

Table 2.   The catalog selected at 3.2 μm

RA[a]	Dec[a]	sub-field	$[3.2]_{ap}$[b] (mag)	$[3.2]_{total}$[c] (mag)
(J2000)				
12 36 44.017	+62 12 50.11	B	17.25 ± 0.15	16.70
12 36 44.626	+62 13 04.29	B	17.46 ± 0.14	16.90
12 36 48.088	+62 13 09.21	B	16.78 ± 0.10	16.51
12 36 49.435	+62 13 46.92	C	15.75 ± 0.04	15.44
12 36 49.541	+62 14 06.85	C	17.57 ± 0.18	17.43
12 36 51.783	+62 13 53.85	C	17.25 ± 0.15	16.99
12 36 53.916	+62 12 54.26	D	17.11 ± 0.11	16.84
12 36 54.742	+62 13 28.01	F	16.80 ± 0.11	16.71
12 36 55.460	+62 13 11.63	F	17.40 ± 0.18	17.07
12 36 56.368	+62 12 41.14	D	17.80 ± 0.21	17.72
12 36 56.675	+62 12 45.51	D	16.85 ± 0.09	16.19

[a]Absolute positions were found with information from the HST/WFPC2 images (Williams et al 1996).

[b]Aperture magnitudes $[3.2]_{ap}$ are measured in a 2.0 arcsec diameter focal-plane aperture.   The quoted uncertainty in magnitude is simply that due to uncertainty in the photon statistics and sky level in the focal-plane aperture. The quoted uncertainty does not take into account uncertainty in overall calibration.

[c]Total magnitudes $[3.2]_{total}$ have been corrected to an effective 6.0 arcsec diameter aperture with information from the H image; see text for details.

Table 3.   Redshifts and colors of the 3.2 μm sources

RA	Dec	$[3.2]_{total}$	z^a	$U - B^b$	$B - V^b$	$V - I^b$	$I - J^b$	$J - H^b$	$H - [3.2]^{b,c}$
(J2000)		(mag)		(mag)	(mag)	(mag)	(mag)	(mag)	(mag)
12 36 44.017	+62 12 50.11	16.70	0.557	−0.17	1.26	1.15	0.66	1.26	1.78
12 36 44.626	+62 13 04.29	16.90	0.485	0.28	1.58	1.29	0.81	1.29	1.78
12 36 48.088	+62 13 09.21	16.51	0.476	1.22	1.93	1.38	0.67	1.23	1.65
12 36 49.435	+62 13 46.92	15.44	0.089	1.46	1.19	0.95	0.56	0.99	0.81
12 36 49.541	+62 14 06.85	17.43	0.752	−0.82	0.96	1.34	0.67	1.24	2.01
12 36 51.783	+62 13 53.85	16.99	0.557	−0.34	1.21	1.21	0.69	1.28	1.73
12 36 53.916	+62 12 54.26	16.84	0.642	−0.55	1.12	1.31	0.68	1.26	1.72
12 36 54.742	+62 13 28.01	16.71	0.000	2.43	1.49	1.19	0.65	0.89	0.58
12 36 55.460	+62 13 11.63	17.07	0.968	73.64	2.26	2.08	1.26	1.37	1.98
12 36 56.368	+62 12 41.14	17.72	0.000	0.76	0.49	0.70	0.48	0.61	−0.04
12 36 56.675	+62 12 45.51	16.19	0.518	1.57	2.04	1.60	0.83	1.29	1.63

[a]Redshifts are from Cohen et al (1996), Lowenthal et al (1997), and Cohen et al (2000). Sources with "0.000" in this column are Galactic stars.

[b]Colors were measured through 2.0 arcsec diameter apertures in images smoothed to match the seeing of the 3.2 μm images; see text. The bandpass names (U, B, V, I, J, H) stand for (F300W,F450W,F606W,F814W,F110W,F160W). Uncertainties in all colors except $(U - B)$ and $(H - [3.2])$ are at or below the 0.01 mag level; see text

[c]Uncertainties in $(H - [3.2])$ color are dominated by the uncertainty in the $[3.2]_{ap}$ magnitude.

Table 4.   Counterparts to the extragalactic 3.2 μm sources

RA	Dec	z	2.15 μm^a	3.2 μm^b	6.7 μm^c	15 μm^c	850 μm^d	8.5 GHz^e	1.4 GHz^e
(J2000)			(μJy)	(μJy)	(μJy)	(μJy)	(μJy)	(μJy)	(μJy)
12 36 44.017	+62 12 50.11	0.557	55.9 ± 3.1	69.2 ± 9.6	< 50	282^{+60}_{-64}	$\cdots$	10.2 ± 1.8	< 23.0
12 36 44.626	+62 13 04.29	0.485	46.5 ± 2.3	57.6 ± 7.4	< 30	33^{+11}_{-15}	3000 ± 600 ?	$\cdots$	$\cdots$
12 36 48.088	+62 13 09.21	0.476	74.3 ± 2.7	82.4 ± 7.6	$\cdots$	$\cdots$	$\cdots$	$\cdots$	$\cdots$
12 36 49.435	+62 13 46.92	0.089	362.5 ± 5.7	220.8 ± 8.1	41^{+66}_{-30}	< 52	$\cdots$	$\cdots$	$\cdots$
12 36 49.541	+62 14 06.85	0.752	21.8 ± 1.5	35.3 ± 5.9	< 40	150^{+74}_{-48}	$\cdots$	$\cdots$	$\cdots$
12 36 51.783	+62 13 53.85	0.557	48.7 ± 2.5	53.0 ± 7.3	< 39	151^{+74}_{-68}	$\cdots$	$\cdots$	$\cdots$
12 36 53.916	+62 12 54.26	0.642	56.9 ± 2.7	60.8 ± 6.2	< 36	179^{+60}_{-43}	$\cdots$	$\cdots$	$\cdots$
12 36 55.460	+62 13 11.63	0.968	39.4 ± 2.4	49.2 ± 8.2	< 37	23^{+10}_{-11}	$\cdots$	12.3 ± 1.8	< 23.0
12 36 56.675	+62 12 45.51	0.518	109.5 ± 4.1	110.7 ± 9.2	$\cdots$	$\cdots$	$\cdots$	$\cdots$	$\cdots$

[a]Flux densities at 2.15 μm are from Hogg et al (2000) converted to Jy under the assumption that $K_s = 0$ mag corresponds to 710 Jy.

[b]Flux densities at 3.2 μm are $[3.2]_{total}$ magnitudes converted under the assumption that $[3.2] = 0$ mag corresponds to 330 Jy.

[c]Flux densities at 6.7 and 15 μm are from Aussel et al (1999).

[d]Flux densities at 850 μm are from Hughes et al (1998). The value is marked with a question mark because there is more than one possible 1.4 GHz counterpart.

[e]Flux densities at 8.5 and 1.4 GHz are from Richards et al (1998) and Richards (1999b).
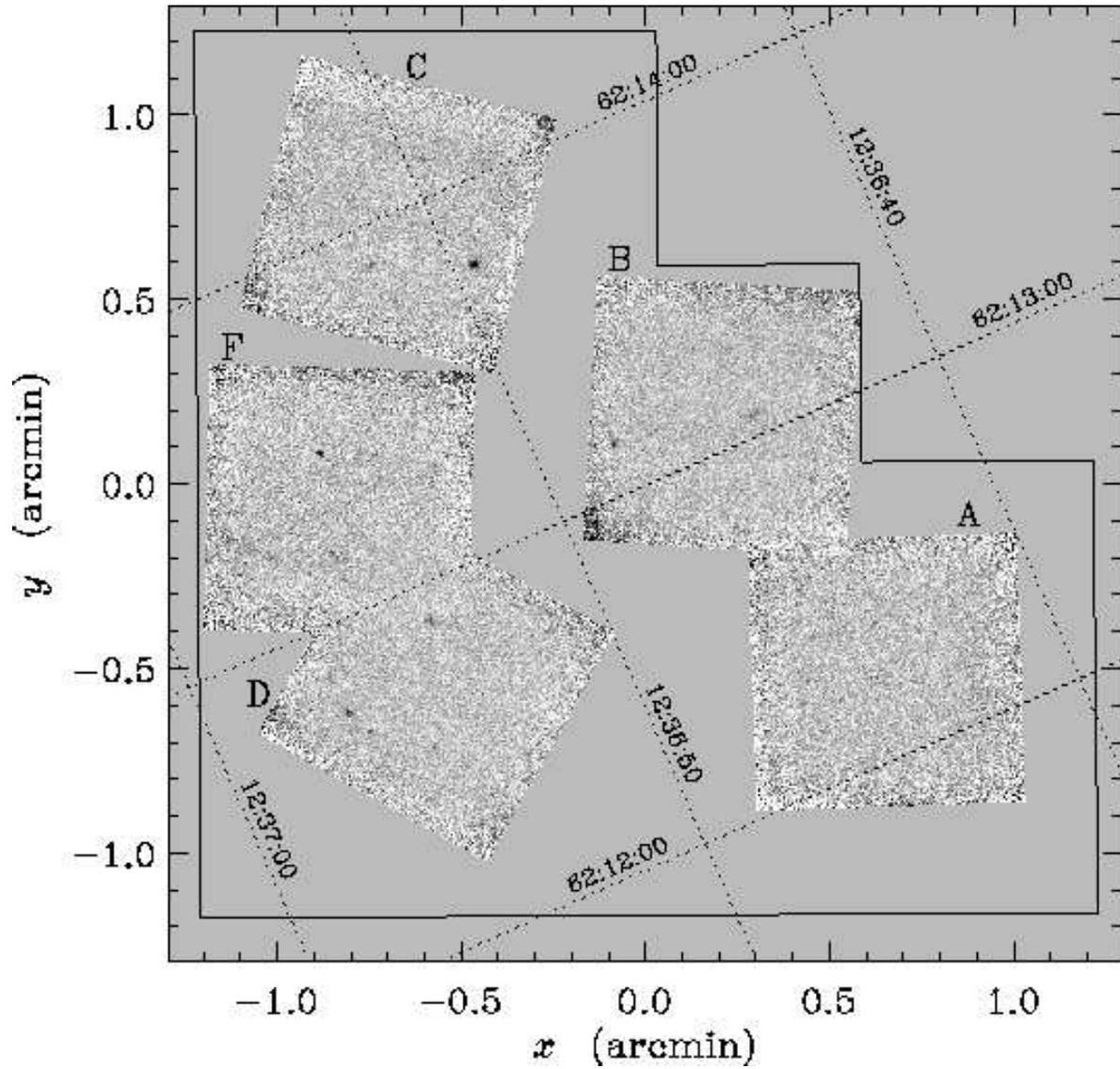
Fig. 1.— The final 3.2 μm mosaic. The subfields are labeled with letters. The outline of the HST–WFPC2 imaged field is shown with a solid line. Lines of constant RA and Dec are shown and labeled.
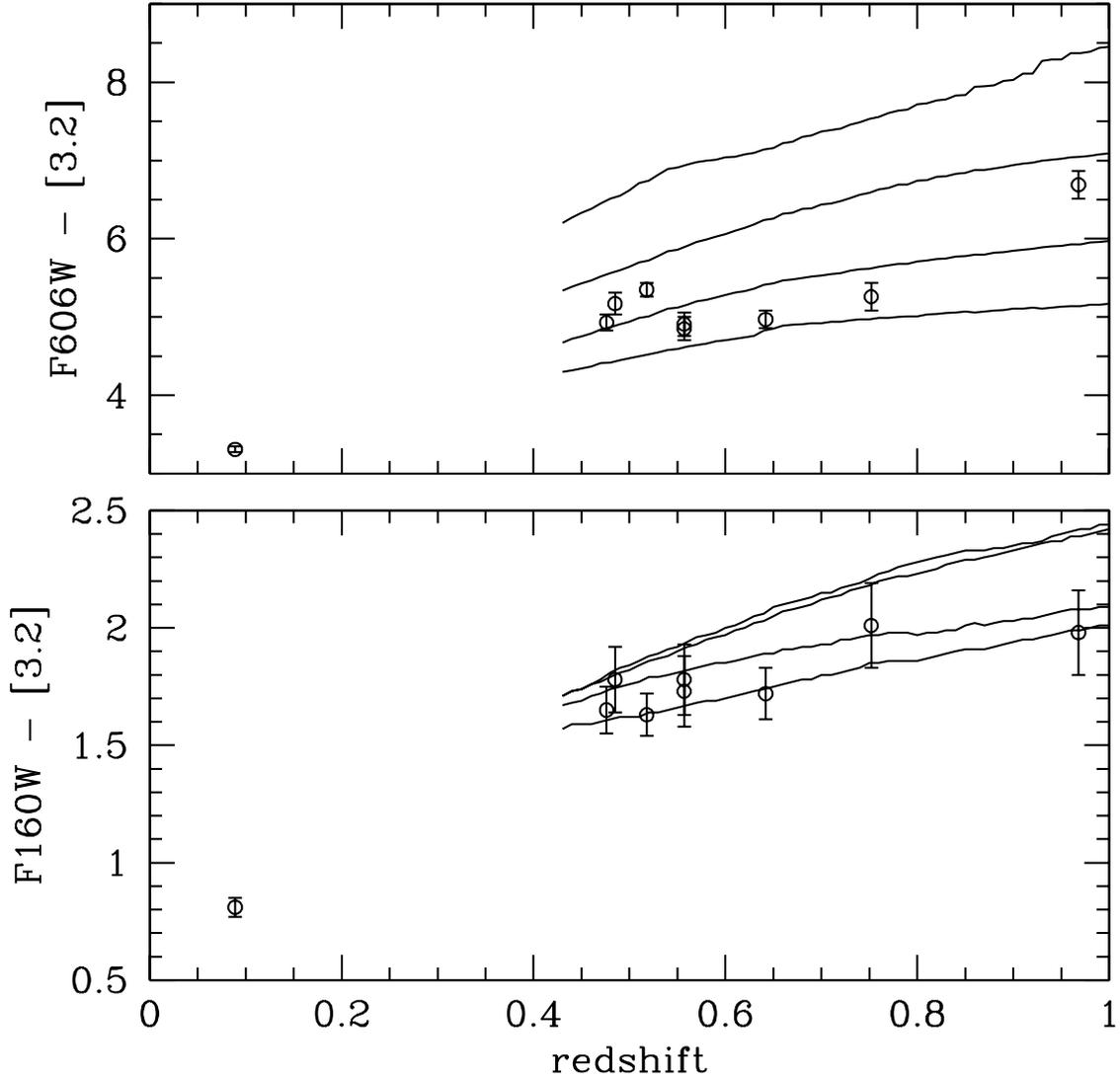
Fig. 2.— The $(V - [3.2])$ and $(H - [3.2])$ colors as a function of redshift for the sources selected at 3.2 μm. Also shown are no-evolution predictions for galaxies of types (from reddest to bluest or top to bottom) E/S0, Sbc, Scd, and Im, based on the bright-galaxy samples of Coleman et al (1980) and Aaronson (1977). The predicted color-redshift tracks begin at redshift $z = 0.43$ because the bright-galaxy data do not extend longward of the K band.
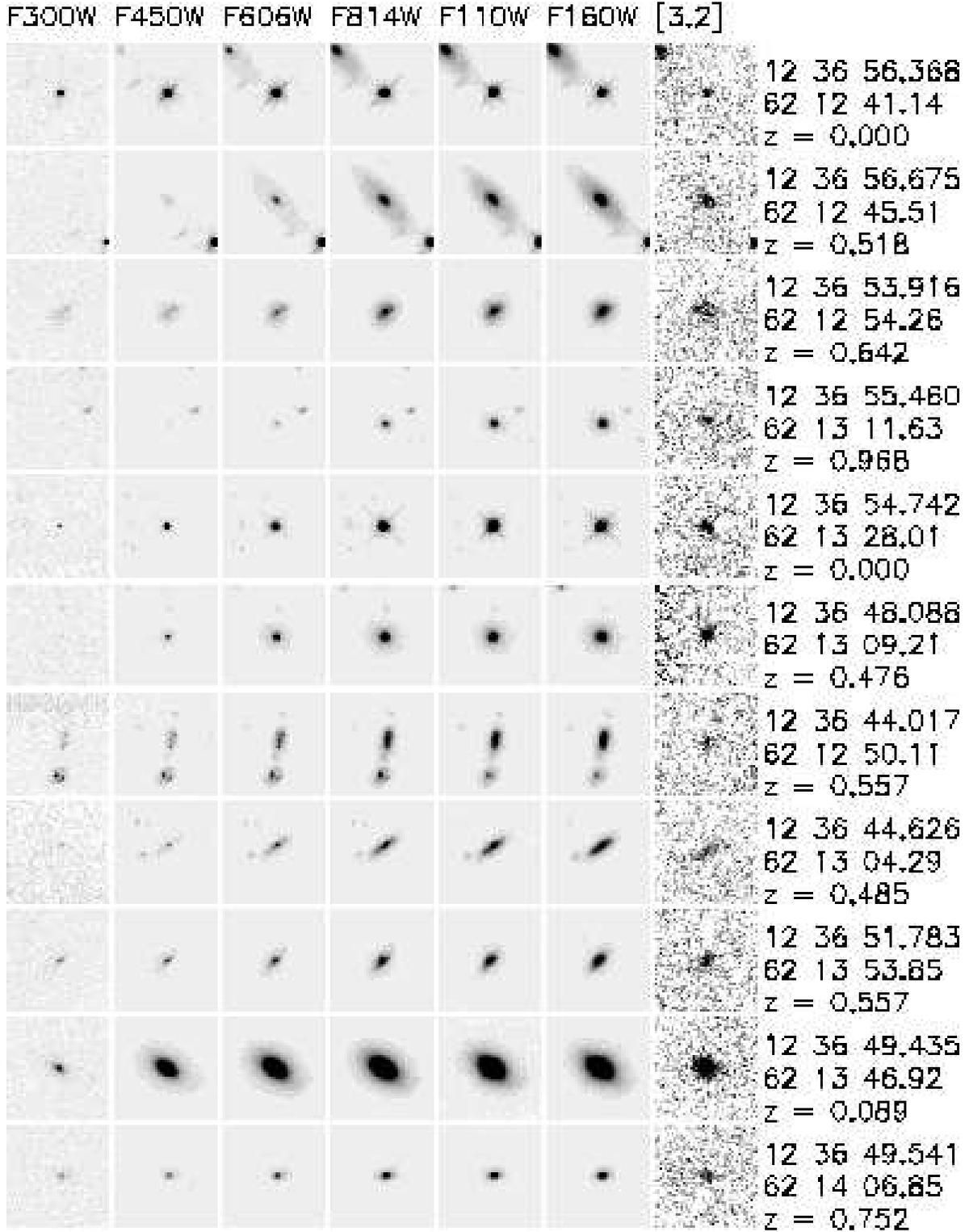
F300W F450W F606W F814W F110W F160W [3.2]

12 36 56.368
62 12 41.14
z = 0.000

12 36 56.675
62 12 45.51
z = 0.518

12 36 53.916
62 12 54.26
z = 0.642

12 36 55.460
62 13 11.63
z = 0.968

12 36 54.742
62 13 28.01
z = 0.000

12 36 48.088
62 13 09.21
z = 0.476

12 36 44.017
62 12 50.11
z = 0.557

12 36 44.626
62 13 04.29
z = 0.485

12 36 51.783
62 13 53.85
z = 0.557

12 36 49.435
62 13 46.92
z = 0.089

12 36 49.541
62 14 06.85
z = 0.752

Fig. 3.— The 2×2 arcsec region around each source selected at 3.2 μm. The images are stretched identically in terms of flux density per logarithmic interval in frequency (νf_ν).